

# Entropy alternatives for equilibrium and out of equilibrium systems

Eugenio E. Vogel<sup>1,2</sup>, Francisco J. Peña<sup>3,\*</sup>, G. Saravia<sup>5</sup> and P. Vargas<sup>3</sup>

<sup>1</sup> *Departamento de Ciencias Físicas, Universidad de La Frontera, Casilla 54-D, Temuco 4811230, Chile*

<sup>2</sup> *Facultad de Ingeniería, Universidad Central de Chile, Santiago 8330601, Chile*

<sup>3</sup> *Departamento de Física, Universidad Técnica Federico Santa María, 2390123 Valparaíso, Chile\* and*

<sup>4</sup> *Los Eucaliptus 1189, Temuco 4812537, Chile*

(Dated: November 1, 2024)

We propose an entropy-related function (non-repeatability) that describes dynamical behaviors in complex systems. A normalized version of this function (mutability) has been previously used in statistical physics. To illustrate their characteristics, we apply these functions to different systems: (a) magnetic moments on a square lattice and (b) real seismic data extracted from the IPOC-2007-2014 catalog. These systems are well-established in the literature, making them suitable benchmarks for testing the new approach. Shannon entropy is used as a reference to facilitate comparison, enabling us to highlight similarities, differences, and the potential benefits of the new measure. Notably, non-repeatability and mutability are sensitive to the order in which the data sequence is collected, distinguishing them from traditional entropy measures.

## I. INTRODUCTION AND BACKGROUND

The concept of entropy ( $S(T)$ ) was enunciated by William Rankine in 1850, followed by definition by Rudolf Clausius in 1865 as the infinitesimal increase of heat concerning an infinitesimal increase in temperature  $T$  [1–6]. The concept of heat can take the form of energy  $E(T)$ , based on energy microstates  $E_i$ , and normalized probability  $p(E_i, T)$  of occupancy of such states. Then, the energy is obtained by adding all the weighted contributions, namely,  $E(T) = \sum_i^{all} E_i p(E_i, T)$ . The partition function can be readily got:  $Z(T) = \sum_i^{all} e^{-E_i/k_B T}$ , with the Boltzmann constant  $k_B$ , which we take as 1.0, to measure energy in units of temperature.

In the Boltzmann-Gibbs statistics the probability  $p(E_i)$  is expressed as  $\exp(-E_i/T)/Z(T)$  which leads to

$$S(T) = - \sum_i^{all} p(E_i, T) \ln(p(E_i, T)). \quad (1)$$

Applications to different systems follow alternative paths. In addition, systems can be in equilibrium or not. The first clear difference is between artificial and natural systems. We will consider here one example of each: Monte Carlo (MC) simulations for spin systems and seismic records for one specific subduction zone. In most of these systems, the states and their probabilities are not completely known (except for tiny systems [7, 8]), so we deal with a sampling of a large universe, usually as a time sequence of records, along some period and recorded with a given numerical precision.

**1) First System: Square spin-lattice.** The energy  $E(T)$  is calculated according to the system's appropriate Hamiltonian. The time evolution will be simulated

by a Monte Carlo protocol in which a random spin (or magnet) is chosen at a time  $t$ , and then it is temporarily flipped. Successive energy differences  $\delta$  (energy before minus energy after the flip) are calculated. If  $\delta$  is negative, the spin-flip is immediately accepted, and  $E(t)$  is updated. If  $\delta$  is positive, the well-known probabilistic Metropolis algorithm is invoked. This process extends over  $20R$  MC steps at each temperature for equilibration. Then, another round of  $20R$  MC steps is done, recording the value of the dependent variable every  $20$  MC steps in a vector file, which at the end holds  $R$  registers. Then, the most probable value of this variable is its average over the  $R$  registers.

**1a) Ising magnets.** In this case, a lattice, like the one illustrated in Fig. 1, is used, where the magnetic moments  $S_{jk}$  can be positive (parallel to the positive  $y$  axis) or negative (opposite direction). Interactions are limited to the nearest neighbors via exchange interactions. The

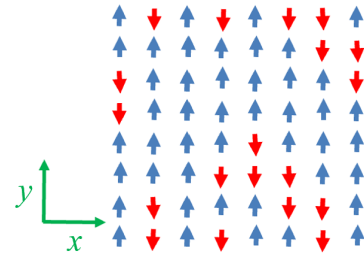


FIG. 1. Geometry of an  $8 \times 8$  lattice on the  $xy$  plane. Magnetic moments can be parallel (upwards) or antiparallel (downwards) to the  $y$  axis. They can represent either Ising spins or strongly anisotropic magnetic dipoles. Their positions are given by the coordinates  $(jk)$ , where  $j = 1, 2, \dots, L$  runs over the  $x$  axis, while  $k = 1, 2, \dots, L$  runs over the  $y$  axis.

\* francisco.penar@usm.cl

Hamiltonian is given by [9–11];

$$H_X = - \sum_{nn} J_{jk,lm} \mathbf{S}_{jk} \cdot \mathbf{S}_{lm}, \quad (2)$$

where the sum extends to all pairs of nearest neighbors (nm) and, for simplicity, all exchange interactions bear the same strength  $J_{jk,lm} = J$ , which is positive for the ferromagnetic interactions considered here. Free boundary conditions will be used, a feature that favors its application to nanoscopic systems [12].

**1b) Dipolar magnets.** Real long narrow magnets (large shape anisotropy) are deposited on the vertexes of a square lattice parallel to the y-axis (in strict correspondence to the geometry of the previous Ising system). These magnets interact via the demagnetizing field produced by each of them. One way to consider log range interaction is via dipole-dipole interactions. The contribution to the Hamiltonian due to a magnet  $\mathbf{S}_{jk}$  interacting with all other magnets  $\mathbf{S}_{lm}$  can be written as [13]:

$$\Delta H_{D,jk} = \frac{\mu_0}{4\pi} \times \sum_{lm} \frac{\mathbf{S}_{jk} \cdot \mathbf{S}_{lm} - 3(\mathbf{S}_{jk} \cdot \hat{\mathbf{r}}_{jk,lm})(\mathbf{S}_{lm} \cdot \hat{\mathbf{r}}_{jk,lm})}{|\mathbf{r}_{jk,lm}|^3}, \quad (3)$$

where  $\mathbf{r}_{jk,lm}$  is the position vector of magnet  $\mathbf{S}_{lm}$  with respect to magnet  $\mathbf{S}_{jk}$  and  $\hat{\mathbf{r}}_{jk,lm}$  is the corresponding unit vector. Then, the total Hamiltonian  $H$  is obtained by adding all  $\Delta H_{D,jk}$  components, taking care of considering each pair of magnets just once. We use the same notation  $\mathbf{S}_{jk}$  to indicate the magnetically active center as in the exchange interactions.

Fig. 1 represents an  $8 \times 8$  lattice which can hold Ising magnetic spins (System 1a) or permanent magnets as dipoles (System 1b) at the vertexes. In both cases, the total number of magnetic states is  $2^N$ , but the way they are dynamically reached (for example, by raising the temperature  $T$ ) is different.

One advantage of the information theory technique is that it recognizes states by matching digits of a number representing state properties. For this purpose, relative values are only needed, so we can take  $J = 1$  for Ising systems and  $\mu_0/(4\pi) = 1$  and the lattice constant equal to 1 unit of length for exchange interactions. Matching digits to recognize states does not need absolute values, but just relative changes in the numeric string.

**2) Second System: California earthquakes.** The USGS (United States Geological Survey) provides a complete catalog of the seisms occurring in the USA [14]. The sequence of seisms with a magnitude over 1.5, depth less than 35 km, and with epicenter within the "rectangle" 115W-119W, 31N-35N was obtained from the USGS, from January 1, 1994, to December 31, 2023. This means 131,459 seisms along these 30 consecutive years.

To illustrate the method, we have collected a subset of 30 seisms from previous data just before and after the Mw 5.25 (5.3) earthquake happening in 2021.06.05. Their magnitudes (down to one decimal point) are listed

in the second column of Table 1.

Table 1: Segment of the data got from the USGS for  $R = 30$  consecutive seisms. The events are enumerated in the first column; the second column (of weight  $w$  bytes) lists the corresponding magnitudes of the earthquakes; next column (of weight  $w^*$  bytes) is the map of the previous column generated by *wlzip*; the fourth column is the frequency  $f_i$  of the corresponding magnitude written in boldface; the fifth column is the relative probability of occurrence of that magnitude  $p_i = f_i/R$ .

$i$	$M_w$	Map generated by <i>wlzip</i>	$f_i$	$p_i$
1	3.8	<b>3.8</b> 0	1	0.033
2	3.0	<b>3.0</b> 1	1	0.033
3	2.4	<b>2.4</b> 2 26	2	0.067
4	2.8	<b>2.8</b> 3, 2 9 16	4	0.133
5	2.8	<b>2.6</b> 5 11 3	3	0.100
6	2.6	<b>2.5</b> 6 15, 2	3	0.100
7	2.5	<b>2.9</b> 7 5 2 3	4	0.133
8	2.9	<b>5.3</b> 8	1	0.033
9	5.3	<b>4.3</b> 9	1	0.033
10	4.3	<b>3.4</b> 10	1	0.033
11	3.4	<b>3.3</b> 11 4	2	0.067
12	3.3	<b>3.5</b> 18	1	0.033
13	2.9	<b>2.1</b> 22 3 2	3	0.100
14	2.8	<b>2.2</b> 23	1	0.033
15	2.9	<b>2.0</b> 24	1	0.033
16	3.3	<b>2.3</b>	1	0.033
17	2.6			
18	2.9			
19	3.5			
20	2.6			
21	2.5			
22	2.5			
23	2.1			
24	2.2			
25	2.0			
26	2.1			
27	2.3			
28	2.1			
29	2.4			
30	2.8			

**Mutability.** Let  $Q(t)$  be a sequence in time  $t$  of parameter  $Q$ . We now consider a segment of  $R$  registers of this sequence ending at time  $t$ . The weight in bytes of this segment is denoted by  $w(Q, R, t)$ . Then, the application of compressor *wlzip* [15] produces a map (third column in Table 1) whose weight in bytes is  $w^*(Q, R)$ . The map is constructed by going through the original file (second column) and opening a new row in the third column for each new value found; this value is written at the beginning of this new row, followed by its distance to the first register of the second column. For later appearances, the distance to the last show is recorded; the number of consecutive appearances is denoted after a coma. The detailed construction of this map has been given in recent papers, [15, 16]. No information is lost since an inverse algorithm can restore the original file  $Q(\nu, t)$ . Then, the mutability associated with this file is

defined as: [7, 8, 17–20]:

$$\zeta(Q, \nu, t) = \frac{w^*(Q, \nu)}{w(Q, \nu, t)}. \quad (4)$$

An alternative information insight can be obtained if the original data file is pre-sorted in ascending or descending order by magnitude. This approach yields the minimum value for mutability, enhancing the identification of critical points, as shown in the results below.

**Functions.** For each system, we report three functions: i) The *non-repeatability*  $V$  given directly by  $w^*$ , namely  $V = w^*$ ; ii) the *mutability*  $\zeta$  defined by Eq. (4); and iii) the *Shannon entropy*  $H = -\sum p_i \ln(p_i)$ , adding over all the states  $i$ . These probabilities are readily given by `wlzip` in the fifth column of Table 1; thus, *the process of getting mutability (as the normalized repeatability) yields  $H$  as a particular case.*

The mutability  $\zeta$  was used in different fields recently [15, 16, 21, 22] and can be interpreted as a dynamical entropy closely related to the Shannon entropy. In the present case, we will compare it to the other functions, in particular with what we have called non-repeatability

## II. RESULTS AND DISCUSSION

Figure 2 presents the non-repeatability results for a data vector for a spin-lattice interacting via exchange interactions. We consider  $R = 1.2 \times 10^5$  records. For larger observational windows (larger  $R$ ), the differences among results for different lattice sizes increase. However, to get exact proportions would require not only larger sampling but also larger lattices (to avoid border effects) and a broader temperature range, which is beyond the scope of the present letter.

Fig. 3 presents the non-repeatability function for the dipolar interaction in three lattice sizes. It is clear that  $V_{L=16}(T) < V_{L=32}(T) < V_{L=64}(T)$ . With a sampling larger than  $1.20 \times 10^5$  registers larger sizes, the differ-

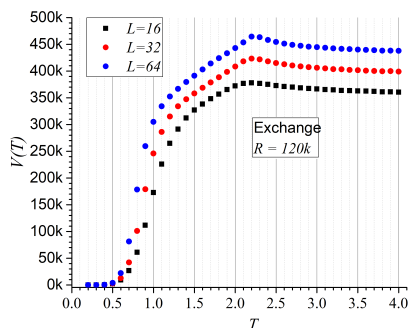


FIG. 2. Average computational entropy  $V(T)$  for exchange interaction only as a function of the temperature  $T$  for three different lattice sizes.  $k$  is the factor 1000.

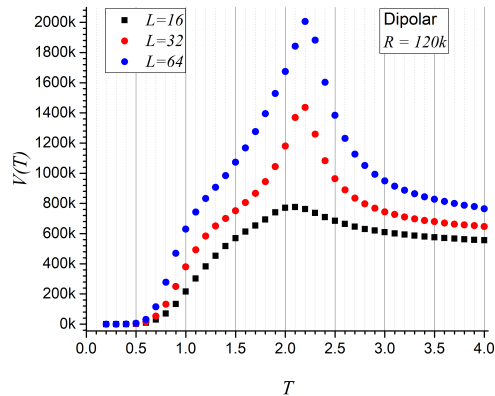


FIG. 3. Average computational entropy  $V(T)$  for the dipolar interaction only for three different lattice sizes as a function of the temperature  $T$ .  $k$  is the factor 1000.

ences among sizes increase. The maximum is also better marked for larger lattices.

In Fig. 4, left panel, we compare Shannon entropy, mutability, and sorted mutability for  $L = 32$  and  $R = 4.8 \times 10^5$  ( $9.6 \times 10^6$  MC steps, after a similar time for equilibration). We used the subsystem with dipolar interactions since it shows less monotonic dependence with  $T$ . Previous conditions apply to the three curves shown in Fig. 4. It should be noticed that different scales are used, but they are adjusted to span the same maximum vertical range in the plot. From Table 1, we already know that Shannon entropy is a byproduct of mutability, so some relationships between them must exist, and sorted mutability originated from the original mutability, so these three curves should exhibit the same general fashion, beginning at zero, growing, maximizing at the critical temperature, descending towards large temperatures. But the ways they vary with temperature reflect the sensitivity of each measurement. Thus, the main advantage of sorted mutability is that its curve is sharper at the critical temperature, pointing to a more precise definition of the values at the critical points.

In the right panel of Fig. 4 we present values of muta-

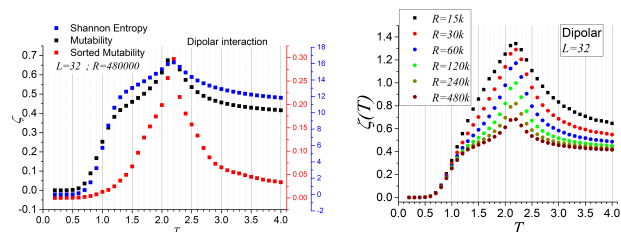


FIG. 4. Left) Shannon entropy, mutability, and sorted mutability for  $L = 32$ , extending the calculations to 480000 registers. Right) Mutability for a lattice with  $L = 32$ , varying  $R$  as given in the inset.  $k$  indicates the factor 1000.

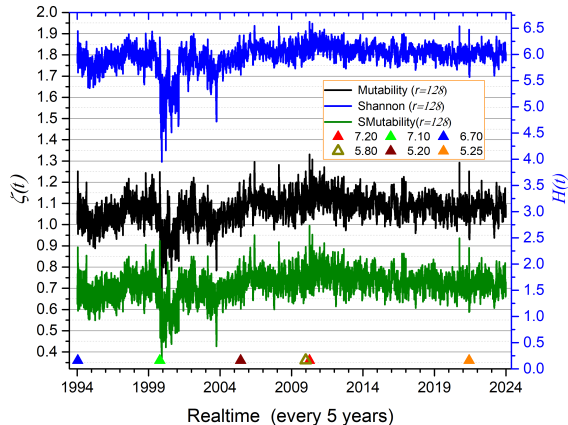


FIG. 5. Shannon entropy, mutability, and sorted mutability for the 131459 earthquakes, from 1994 to 2023, with magnitude  $M_w \geq 1.5$ , up to 30 km depth, with an epicenter in the rectangle near Los Angeles and San Diego defined in the text. Time for important seisms is marked by the symbols defined in the inset.

bility for the same parameters used for the left panel but for different observation windows  $R$ , as given in the inset. Actually, the lower curve on the right is the same mutability curve (black) on the left. We can see that there are negligible differences for low  $T$ , but the maximum value decreases rapidly with larger observation times. As temperatures increase, the mutability of all curves decreases, eventually reaching saturation. It can be expected that this tendency will hold ending with the classical entropy curve in the thermodynamic limit: a slightly ascending curve, going through an inflection point, and finally tending asymptotically to saturation at extremely high temperatures. Partial tests done for larger lattices (not shown) confirm and reinforce these observations. Then, the maximum reached by the curves in Fig. 4 is an artifact of the finite size of the observation time, disappearing with larger  $R$  values. However,  $R$  can be tuned to provide accurate information on critical phenomena.

Finally, we turn our attention to the seismic activity of the Los Angeles/San Diego area in California. In Fig. 5, we give the results for Shannon entropy, mutability, and sorted mutability for mobile overlapping time windows of  $r = 128$  consecutive events (the overlap is in one element of the sequence). Ordinate axes have been adjusted so the three curves exhibit a similar maximum vertical span ( $\approx 0.65$  measured on the left vertical axis, between the maxima in 2012 and the respective minimum in 2000).

The first observation is the similarity of these curves, confirming that Shannon entropy and mutability are related. Second, major earthquakes tend to show upward

“needles”, but the opposite is not always true: there are vertical needles not corresponding to single large earthquakes, a point that should be further investigated focusing on local behavior and swarms of seisms. Third, the undulations of the general trend are better shown by the mutability curves. Fourth, the mutability curves better show the span of the downward behavior corresponding to the aftershock regimes. Fifth, the mutability curves exhibit more texture (larger amplitudes and better definition of consecutive lines) than the curve for Shannon entropy. Sixth, sorted mutability gives more details than plain mutability: see, for instance, the definition in the upward needles around the year 2010.

### III. CONCLUSIONS

Non-repeatability  $V(T)$  grows with the number of elements (lattice size), although finite equilibration and observation times are not yet enough to fully appreciate if this behavior leads to additivity.

Previous conclusions hold both for exchange interactions and dipolar interactions. However, they are more notorious for the latter, probably because of the richer dynamics caused by the long-range interactions.

Normalized non-repeatability or mutability includes Shannon entropy as a particular case when the map generated by the data compressor (wzip) reduces to the probabilities of different states appearing in the sampling. This is appreciated because mutability is always under the Shannon entropy plots in the spin systems, thus allowing for a more precise reading of the maxima at the critical point. This maximum of mutability at the critical point is an artifact of the finite times of observation.

Both mutability and Shannon entropy allow us to analyze seismic activity. Upward needles in Fig. 5 are due to large earthquakes or swarms of several moderate earthquakes. By the same token, low values of these two parameters describe the aftershock regime produced by large earthquakes caused by the repetition of lower magnitude values.

Sorted mutability, both in spin systems and earthquake analysis, gives more texture and finer definition on the critical points than plain mutability.

Mutability, in both forms, has advantages regarding Shannon entropy. It shows more contrast in the undulations, more texture in the fine description of the seism sequence, and more recognition of aftershock regimes.

### ACKNOWLEDGEMENTS

Authors acknowledge partial support from ANID Fondecyt Grant (Chile) under contracts 1230055 and 1240582.

[1] C. Tsallis, Entropy, Encyclopedia **2**, 264 (2022).

[2] A. Wehrl, General properties of entropy, Reviews of Modern Physics **50**, 221 (1978).

- [3] W. Greiner, L. Neise, and H. Stöcker, *Thermodynamics and statistical mechanics* (Springer Science & Business Media, 2012).
- [4] H. B. Callen and H. Scott, *Thermodynamics and an introduction to thermostatistics* (1998).
- [5] E. Zanchini and G. P. Beretta, Recent progress in the definition of thermodynamic entropy, *Entropy* **16**, 1547 (2014).
- [6] E. P. Gyftopoulos *et al.*, Entropy: Thermodynamic definition and quantum expression, *Physical Review E* **55**, 3851 (1997).
- [7] O. A. Negrete, P. Vargas, F. J. Peña, G. Saravia, and E. E. Vogel, Entropy and mutability for the q-state clock model in small systems, *Entropy* **20**, 933 (2018).
- [8] O. A. Negrete, P. Vargas, F. J. Peña, G. Saravia, and E. E. Vogel, Short-range berezinskii-kosterlitz-thouless phase characterization for the q-state clock model, *Entropy* **23**, 1019 (2021).
- [9] G. F. Newell and E. W. Montroll, On the theory of the ising model of ferromagnetism, *Reviews of Modern Physics* **25**, 353 (1953).
- [10] G. Joyce, Classical heisenberg model, *Physical Review* **155**, 478 (1967).
- [11] M. Takahashi, One-dimensional heisenberg model at finite temperature, *Progress of Theoretical Physics* **46**, 401 (1971).
- [12] E. E. Vogel, P. Vargas, G. Saravia, J. Valdes, A. J. Ramirez-Pastor, and P. M. Centres, Thermodynamics of small magnetic particles, *Entropy* **19**, 499 (2017).
- [13] K. De'Bell, A. MacIsaac, and J. Whitehead, Dipolar effects in magnetic thin films and quasi-two-dimensional systems, *Reviews of Modern Physics* **72**, 225 (2000).
- [14] USGS, <https://earthquake.usgs.gov/earthquakes/search/usgs> (2024).
- [15] D. Pasten, E. E. Vogel, G. Saravia, A. Posadas, and O. Sotolongo, Tsallis entropy and mutability to characterize seismic sequences: The case of 2007–2014 northern chile earthquakes, *Entropy* **25**, 1417 (2023).
- [16] E. Vogel, G. Saravia, S. Kobe, and R. Schuster, Onshore versus offshore capacity factor and reliability for wind energy production in germany: 2010–2022, *Energy Science & Engineering* **12**, 2198 (2024).
- [17] E. Vogel, G. Saravia, and A. J. Ramirez-Pastor, Phase transitions in a system of long rods on two-dimensional lattices by means of information theory, *Physical Review E* **96**, 062133 (2017).
- [18] E. Vogel, G. Saravia, D. Pastén, and V. Muñoz, Time-series analysis of earthquake sequences by means of information recognizer, *Tectonophysics* **712**, 723 (2017).
- [19] E. Vogel, G. Saravia, S. Kobe, R. Schumann, and R. Schuster, A novel method to optimize electricity generation from wind energy, *Renewable Energy* **126**, 724 (2018).
- [20] E. E. Vogel, F. G. Brevis, D. Pastén, V. Muñoz, R. A. Miranda, and A. C.-L. Chian, Measuring the seismic risk along the nazca–south american subduction front: Shannon entropy and mutability, *Natural Hazards and Earth System Sciences* **20**, 2943 (2020).
- [21] E. Vogel, G. Saravia, A. J. Ramirez-Pastor, and M. Pasinetti, Alternative characterization of the nematic transition in deposition of rods on two-dimensional lattices, *Physical Review E* **101**, 022104 (2020).
- [22] R. Caitano, A. Ramirez-Pastor, E. Vogel, and G. Saravia, Competition analysis of grain flow versus clogging by means of information theory, *Granular Matter* **26**, 77 (2024).